Supplementary Material

Exposure and Toxicity Characterization of Chemical Emissions and Chemicals in Products: Global Recommendations and Implementation in USEtox

Peter Fantke[1*], Weihsueh A. Chiu[2], Lesa Aylward[3], Richard Judson[4], Lei Huang[5], Suji Jang[2], Todd Gouin[6], Lorenz Rhomberg[7], Nicolò Aurisano[1], Thomas McKone[8], Olivier Jolliet[5]

[1] Quantitative Sustainability Assessment, Department of Technology, Management and Economics, Technical University of Denmark, Produktionstorvet 424, 2800 Kgs. Lyngby, Denmark

[2] Department of Veterinary Integrative Biosciences, College of Veterinary Medicine and Biomedical Sciences, Texas A&M University, College Station, Texas, USA

[3] Queensland Alliance for Environmental Health Sciences, University of Queensland, Brisbane, Australia

[4] National Center for Computational Toxicology, U.S. Environmental Protection Agency, Research Triangle Park, NC 27711, USA

[5] Department of Environmental Health Sciences, School of Public Health, University of Michigan, Ann Arbor, Michigan 48109, USA

[6] TG Environmental Research, Sharnbrook, MK44 1PL, UK

[7] Gradient, Boston, Massachusetts 02108, USA

[8] School of Public Health, University of California, Berkeley, California 94720, USA

[*]Corresponding author: Tel.: +45 45254452, fax: +45 45933435. E-mail: pefan@dtu.dk

Table of Contents

S-1 Near-field exposure assessment

The calculation of direct chemical mass transfer fractions from the consumer product to environmental and human compartments requires physiochemical properties as input, including molecular weight, vapor pressure, water solubility, and air-water and octanol-water partition coefficients, obtained from various sources (e.g. Sobanska & Le Goff 2014, Williams et al. 2017), with a preference for experimental data when available. Enthalpies of vaporization, predicted using the ACD/Labs Percepta Platform, are available from Williams (2011). Further required inputs including diffusion coefficients in solid materials, material-air, material-water partition coefficients, and skin permeation coefficients are obtained from quantitative property-property relationships (QPPRs) (see Table S1), as well as material-dust partition coefficients (set to 1, assuming surface dust originates in abrasion of solid materials). We recommend to use empirical data, specifically in cases where QPPR predictions are not available or applicable, such as for per- and polyfluoroalkyl substances (PFAS).
Calculating direct transfer fractions also requires input on room characteristics and exposure scenario settings. Characteristics of a typical OECD household are used as reference scenario (Little et al. 2012, Rosenbaum et al. 2015, Wenger et al. 2012), assuming two adults and one child per household, and with values for exposure factors (e.g. inhalation rate) for adults and children obtained from several sources (Csiszar et al. 2017, Little et al. 2012, US-EPA 2011). Additional, product-type-specific parameters (e.g. area and thickness of articles, area, thickness and density of products applied on skin surface) are obtained from several references (Bremmer et al. 2006, Cox et al. 2002, Csiszar et al. 2017, Csiszar et al. 2016, Isaacs et al. 2014, Meesters et al. 2018, US-EPA 2011, Wenger et al. 2012). For details on reference scenario settings and product-related parameters for all models calculating direct transfer fractions see Tables S2 and S3.

Table S1. Key physicochemical properties, corresponding property-property relationships (QPPR) and their input parameters, as input to models calculating direct transfer fractions.

Property	QPPR used	Input parameters
Diffusion coefficient	Huang et al. (2017) is used to derive the chemical diffusion coefficients in different building materials from molecular weight, temperature and the material type ($R^2_{\text{adj}} = 0.93$): $\log D_m - \frac{\tau - 3486}{T} = 6.39 - 2.49 \times \log MW + b$	D_m [m²/s] is the diffusion coefficient, MW [g/mol] is the molecular weight, T [K] is temperature, b and τ are material-specific coefficients available for 32 materials
Material-air partition coefficient	Huang and Jolliet (2019a) is used to derive the material-air partition coefficient K_{ma} of target chemicals in different building materials from octanol-air partition coefficient, enthalpy of	K_{oa} is the dimensionless octanol-air partition coefficient derived from EPISuite, $R =$ 8.314 J/mol/K is the ideal gas

Property	QPPR used	Input parameters
	vaporization, temperature and the material type ($R^2_{adj} = 0.93$): $\log K_{ma} = -0.38 + 0.63 \times \log K_{oa} + 0.96 \times \frac{\Delta H_{ma}}{2.303 \times R} \times \left(\frac{1}{T} - \frac{1}{298.15}\right) + \beta$ A more generic but slightly less accurate relationship can be used to derive K_{ma} for materials without available β coefficient ($R^2_{adj} = 0.84$): $\log K_{ma} = -0.37 + 0.75 \times \log K_{oa} + 1.29 \times \frac{\Delta H_{ma}}{2.303 \times R} \times \left(\frac{1}{T} - \frac{1}{298.15}\right)$	constant, β is a material-specific coefficient available for 22 materials, ΔH_{ma} [kJ/mol] is the enthalpy of phase change between material and air, and is derived from the enthalpy of vaporization ΔH_v [kJ/mol] by ($R^2_{adj} = 0.78$): $\Delta H_{ma} = 1.37 \times \Delta H_v - 14$
Packaging-food and material-water partition coefficients	Huang and Jolliet (2019b) is used to derive the packaging-food partition coefficient K_{pf} (with material-water partition coefficient being a particular case of K_{pf}) of target chemicals in different packaging materials from octanol-water partition coefficient, food/water ethanol equivalency, temperature and the material type ($R^2_{adj} = 0.93$): $\log K_{pf} = -1.36 + 1.06 \times \log K_{ow} - 0.014 \times EtOH_{eq} - 0.0066 \times \log K_{ow} \times EtOH_{eq} + 866 \times \left(\frac{1}{T} - \frac{1}{298.15}\right) + \beta$ A more generic but slightly less accurate relationship can be used to derive K_{pf} for materials without available β coefficient ($R^2_{adj} = 0.9$): $\log K_{pf} = -1.96 + 1.16 \times \log K_{ow} - 0.059 \times EtOH_{eq} - 0.0079 \times \log K_{ow} \times EtOH_{eq} + 805 \times \left(\frac{1}{T} - \frac{1}{298.15}\right)$	K_{ow} [L/L] is the octanol-water partition coefficient derived from EPISuite, $EtOH_{eq}$ [%] is the ethanol equivalency of food expressed as a percentage of ethanol in water in terms of volume/volume ratio whose value ranges from 0% to 100% (0% for water)
Skin permeation coefficients	The methods from ten Berge (2009) as applied by Csiszar et al. (2017) are used to derive the skin permeation coefficient via aqueous solution $K_{p\text{-}aq}$ [m/s] and the total gaseous-skin permeation coefficient $K_{p\text{-}gas}$ [m/s]: $K_{p\text{-}aq} = 2.78 \times 10^{-6} \times \left(\frac{0.043}{MW^{1.361}} + 10^{0.7318 \times \log K_{ow} - 0.00683 \times MW - 2.59}\right)$ $K_{p\text{-}gas} = \frac{1}{\frac{K_{aw,T}}{K_{p\text{-}aq}} + \frac{1}{v_a}}$	v_a is the air flow rate over the body surface area, which is set to 0.00278 m/s by default, $K_{aw,T}$ is the dimensionless air-water partition coefficient at the specified temperature, MW [g/mol] is the molecular weight

Reference household characteristics, exposure factors and product-type-specific exposure scenario settings are constructed from a set of representative nominal values listed in Table S2, while stochastic modelling could also be applied to determine parameter and results distributions and quantify related uncertainties.

Table S2. Default household characteristics, exposure factors and exposure scenario settings for different product types.

Parameter	Value	Unit	Reference
Indoor configuration			
Room volume (V)	236	m^3	Rosenbaum et al. (2015) (OECD countries)
Room air renewal rate (n)	0.79	h^{-1}	Rosenbaum et al. (2015) (OECD countries).
Convective mass-transfer coefficient (h_m, h_s)	0.0024	m/s	Wenger et al. (2012) (Table 1)
Total suspended particle concentration (TSP)	20	$\mu g/m^3$	Little et al. (2012) (Table S1)
Density of airborne particles (ρ_{part})	1E+12	$\mu g/m^3$	Little et al. (2012) (Table 1)
Density of settled dust (ρ_{dust})	1E+09	mg/m^3	Little et al. (2012) (Table 1)
Exposure factors			
Number of children (N_child)	1	-	Own assumption
Number of adult (N_adult)	2	-	Own assumption
Inhalation rate, 2-3 year old (inhR_c)	8.9	m^3/d	US-EPA (2011) (Table 6-1)
Inhalation rate, adult (inhR_a)	16	m^3/d	US-EPA (2011) (Table 6-1)
Body weight, 2-3 year old (BW_c)	13.8	kg	US-EPA (2011) (Table 8-1)
Body weight, adult (BW_a)	70	kg	Rosenbaum et al. (2011) (Table S3)
Dust ingestion rate, 2-3 year old (ingR_c)	59.34	mg/d	Little et al. (2012) (Table 2)
Dust ingestion rate, adult (ingR_a)	60	mg/d	Little et al. (2012) (Table 2)
Time spent at home, 2-3 year old (f_indoor_c)	979	min/d	US-EPA (2011) (Table 16-1)
Time spent at home, 18-65 years adult (f_indoor_a)	948	min/d	US-EPA (2011) (Table 16-1)

Product-related data that are used as input to models calculating direct transfer fractions are summarized in Table S3, provided in a separate file.

S-2 Supplement for product-related models

S-2a Article interior partition-limited model with indoor sorption

In this model, we assume that the chemical is always evenly distributed inside a given product and sorption material, i.e. there is no concentration gradient through the materials. The mass balance equations are as follows:

$$\frac{dm_m(t)}{dt} = -\left(\frac{m_m(t)}{A_m \cdot L_m}/K_{ma} - \frac{m_a(t)}{V \cdot (1+K_{pa} \cdot TSP)}\right) \cdot h_m \cdot A_m \quad \text{(S1)}$$

$$\frac{dm_s(t)}{dt} = \left(\frac{m_a}{V \cdot (1+K_{pa} \cdot TSP)} - \frac{m_s}{A_s \cdot L_s}/K_s\right) \cdot h_s \cdot A_s \quad \text{(S2)}$$

where m_m is the chemical mass in a given product material (µg), m_s is the chemical mass in a sorption material (µg), A_s is the area of sorption surfaces (m^2), L_s is the thickness of indoor surface materials (m), K_s is the chemical's sorption material-air partition coefficient (−), h_s is the convective mass-transfer coefficient on the sorption surfaces (m/s). Since the kinetic of

indoor air is much faster than the kinetic from emitting and adsorbing surfaces, it equilibrates between these masses and we assume a quasi-steady-state for the chemical in indoor air:

$$\frac{dm_a(t)}{dt} = \left(\frac{m_m(t)}{A_m \cdot L_m}/K_{ma} - \frac{m_a(t)}{V \cdot (1+K_{pa} \cdot TSP)}\right) \cdot h_m \cdot A_m - \left(\frac{m_a}{V \cdot (1+K_{pa} \cdot TSP)} - \frac{m_s}{A_s \cdot L_s}/K_s\right) \cdot h_s \cdot A_s - n \cdot m_a \approx 0 \quad \text{(S3)}$$

$$\text{thus, } m_a(t) = \left(\frac{m_m \cdot h_m}{L_m \cdot K_{ma}} + \frac{m_s \cdot h_s}{L_s \cdot K_s}\right) \cdot \left(n + \frac{h_s \cdot A_s + h_m \cdot A_m}{V \cdot (1+K_{pa} \cdot TSP)}\right)^{-1} \quad \text{(S4)}$$

where m_a is the chemical mass in indoor air gas and particle phases (µg), and $n = Q/V$ is the air renewal rate (s^{-1}), with Q as ventilation rate (m^3/s) and V as room volume (m^3). Replacing $m_a(t)$ in equations S1 and S2, the mass balance equation can be expressed in matrix notation as follows:

$$\boldsymbol{M}'(t) = \mathbf{A_k}\, \boldsymbol{M}(t) \quad \text{(S5)}$$

with

$$\boldsymbol{M}(t) = \begin{bmatrix} m_m(t) \\ m_s(t) \end{bmatrix}, \text{ and}$$

$$\mathbf{A_k} = \begin{bmatrix} -\frac{h_m}{L \cdot K_{ma}} + \frac{h_m^2 \cdot A_m}{L \cdot K_{ma}} \cdot \frac{1}{Q \cdot (1+K_{pa} \cdot TSP) + h_m \cdot A_m + h_s \cdot A_s} & \frac{h_m \cdot A_m \cdot h_s}{L_s \cdot K_s} \cdot \frac{1}{Q \cdot (1+K_{pa} \cdot TSP) + h_m \cdot A_m + h_s \cdot A_s} \\ \frac{h_s \cdot A_s \cdot h_m}{L \cdot K_{ma}} \cdot \frac{1}{Q \cdot (1+K_{pa} \cdot TSP) + h_m \cdot A_m + h_s \cdot A_s} & -\frac{h_s}{L_s \cdot K_s} + \frac{h_s^2 \cdot A_s}{L_s \cdot K_s} \cdot \frac{1}{Q \cdot (1+K_{pa} \cdot TSP) + h_m \cdot A_m + h_s \cdot A_s} \end{bmatrix}$$

The solution of equation S5 is:

$$\boldsymbol{M}(\boldsymbol{t}) = c_1 e^{\lambda_1 t} \mathbf{u_1} + c_2 e^{\lambda_2 t} \mathbf{u_2} \quad \text{(S6)}$$

$$\begin{bmatrix} c_1 \\ c_2 \end{bmatrix} = [\boldsymbol{u_1}\ \boldsymbol{u_2}]^{-1}\, \boldsymbol{M}(\mathbf{0}) = [\boldsymbol{u_1}\ \boldsymbol{u_2}]^{-1} \begin{bmatrix} m_m(0) \\ m_s(0) \end{bmatrix} \quad \text{(S7)}$$

where λ_1 and λ_2 are the two eigenvalues of matrix $\mathbf{A_k}$, $\boldsymbol{u_1}$ and $\boldsymbol{u_2}$ are the respective eigenvectors of $\mathbf{A_k}$, and c_1 and c_2 are constants. After obtaining $m_m(t)$ and $m_s(t)$ by equation S6, the direct transfer fraction from a given material to indoor air from time zero to time t (s) is given by:

$$TF_{ma} = 1 - \frac{m_m(t)}{m_0} \quad \text{(S8)}$$

S-2b Rate constants for the skin surface layer model

$$k_{hm} = -FQ_{hm} \cdot \ln(1 - TE_{hm});\ k_{pa} = \left(\frac{1}{v_{iw}} + \frac{1}{v_a \cdot K_{aw\_T}}\right)^{-1} \cdot \frac{1}{L};\ k_{ps} = \left(\frac{1}{v_{iw}} + \frac{1}{K_{p\_aq}}\right)^{-1} \cdot \frac{1}{L}$$

where k_{hm} is the hand-to-mouth rate constant (hr^{-1}), k_{pa} is the product-air transfer rate constant (hr^{-1}), and k_{ps} is the product-skin transfer rate constant (hr^{-1}), with FQ_{hm} as hand-to-mouth contact frequency (events/hr), TE_{hm} as hand-to-mouth removal efficiency (assumed to be 0.5), v_{iw} as water-side mass transfer coefficient (cm/hr), v_a as air flow rate over the body surface area (1000 cm/hr), K_{aw_T} as air-water partitioning coefficient at specified

temperature (−), L as product material thickness (cm), and K_{p_aq} as aqueous dermal permeation coefficient (cm/hr).

S-2c Rate constants for the object surface model

$$k_{NS\rightarrow NA} = \frac{\varphi_{\text{water-air}}}{L_{OS}};\ k_{NS\rightarrow\text{skin}} = \frac{K_p}{\frac{AR}{1000}\cdot\frac{A_{NP}}{A_{\text{skin}}}};\ k_{NS\rightarrow FS} = \frac{1}{t_{\text{app}}\cdot\frac{A_{NP}}{A_{\text{total}}}};\ k_{NS,\text{deg}} = k_{\text{deg,surf}}$$

where $k_{NS\rightarrow NA}$ is the near-person surface to near-person air transfer rate constant (hr^{-1}), $k_{NS\rightarrow\text{skin}}$ is the near-person surface to skin transfer rate constant (hr^{-1}), $k_{NS\rightarrow FS}$ is the near-person surface to far-person surface transfer rate constant (hr^{-1}), and $k_{NS,\text{deg}}$ is the near-person surface degradation rate constant (hr^{-1}), with $\varphi_{\text{water-air}}$ as mass transfer velocity from water to air (m/hr), L_{OS} as thickness of the liquid layer of a product on the object surface (m), AR as application rate of a product (L/m^2), A_{NP} as near-person area (0.5 m^2) (Earnest & Corsi 2013), A_{skin} as dermal contact area during product application (m^2), A_{total} as total area of the product application (m^2), t_{app} as duration of the product application (hr), and $k_{\text{deg,surf}}$ as the chemical's surface degradation rate constant (hr^{-1}).

S-2d Indoor sorption model

For indoor sorption as process relevant for all product-specific models, we assume that once the chemical is adsorbed on indoor sorption materials, it will always be evenly distributed inside the sorption materials, i.e. there is no concentration gradient through the materials. The mass balance equations are as follows:

$$\frac{dm_a(t)}{dt} = -\left(\frac{m_a}{V\cdot(1+K_{pa}\cdot TSP)} - \frac{m_s(t)}{A_s\cdot L_s\cdot K_s}\right)\cdot h_s\cdot A_s - \frac{m_a}{V\cdot(1+K_{pa}\cdot TSP)}\cdot K_{p,\text{gas,total}}\cdot\left(A_{\text{skin,gas},a}\cdot N_{\text{adult}} + A_{\text{skin,gas},c}\cdot N_{\text{child}}\right) - n\cdot m_a \quad \text{(S9)}$$

$$\frac{dm_s(t)}{dt} = \left(\frac{m_a}{V\cdot(1+K_{pa}\cdot TSP)} - \frac{m_s(t)}{A_s\cdot L_s\cdot K_s}\right)\cdot h_s\cdot A_s \quad \text{(S10)}$$

where m_a is the chemical mass in indoor air (µg), m_s is the chemical mass in the sorption material (µg), A_s is the area of indoor sorption surfaces (m^2), L_s is the thickness of indoor sorption materials (m), K_s is the chemical's sorption material-air partition coefficient (−), h_s is the convective mass-transfer coefficient on indoor sorption surfaces (m/s), $K_{p,\text{gas,total}}$ is the total gaseous-skin permeation coefficient (m/s), K_{pa} is the chemical's particle-air partition coefficient ($\text{m}^3/\mu\text{g}$), TSP is the total suspended particle concentration ($\mu\text{g/m}^3$), $A_{\text{skin,gas},a}$ is the skin gaseous uptake area for adults (m^2), $A_{\text{skin,gas},c}$ is the skin gaseous uptake area for children (m^2), N_{adult} is the number of considered adults, N_{child} is the number of considered children, and

n is the air renewal rate (s^{-1}). The above two mass balance equations equation can be expressed in matrix notation as follows:

$$\boldsymbol{M}'(t) = \mathbf{A_k}\,\boldsymbol{M}(t) \quad \text{(S11)}$$

with

$$\boldsymbol{M}(t) = \begin{bmatrix} m_a(t) \\ m_s(t) \end{bmatrix}, \text{ and}$$

$$\mathbf{A_k} = \begin{bmatrix} -\frac{h_s \cdot A_s}{V(1+K_{pa} \cdot TSP)} - \frac{K_{p\_gas\_total}}{V(1+K_{pa} \cdot TSP)} \cdot \left(A_{skin,gas,a} \cdot N_{adult} + A_{skin,gas,c} \cdot N_{child}\right) - n & \frac{h_s}{L_s \cdot K_s} \\ \frac{h_s \cdot A_s}{V(1+K_{pa} \cdot TSP)} & -\frac{h_s}{L_s \cdot K_s} \end{bmatrix}$$

The solution of equation S11 is:

$$\boldsymbol{M(t)} = c_1 e^{\lambda_1 t}\mathbf{u_1} + c_2 e^{\lambda_2 t}\mathbf{u_2} \quad \text{(S12)}$$

$$\begin{bmatrix} c_1 \\ c_2 \end{bmatrix} = [\boldsymbol{u_1}\ \boldsymbol{u_2}]^{-1}\,\boldsymbol{M(0)} = [\boldsymbol{u_1}\ \boldsymbol{u_2}]^{-1} \begin{bmatrix} m_a(0) \\ m_s(0) \end{bmatrix} \quad \text{(S13)}$$

where λ_1 and λ_2 are the two eigenvalues of matrix $\mathbf{A_k}$, $\boldsymbol{u_1}$ and $\boldsymbol{u_2}$ are the respective eigenvectors of $\mathbf{A_k}$, and c_1 and c_2 are constants. $m_a(0)$ is the initial chemical mass in indoor air and is assumed to be 100 mg (an arbitrary value, which does not influence the calculation of transfer fractions), and $m_s(0)$ is the initial chemical mass in indoor sorption material, which is zero. Finally, the direct transfer fraction from indoor air to indoor sorption materials from time zero to time t (s) is given by:

$$TF_{\text{sorption}} = \frac{m_s(t)}{m_a(0)} \quad \text{(S14)}$$

S-3 Human dose-response modelling

S-3a Identifying points of departure (POD)

If for a given chemical, regulatory assessment-based data are not available, the next POD source is experimental animal data. Specifically, with the emergence of large experimental animal databases both in the U.S. (e.g. ToxValDB) and the EU (e.g. REACH dossiers), it is possible to obtain experimental animal-based PODs for a large number of chemicals, following careful data curation where needed (Fantke et al. 2020), or apply a statistical approach across data from different animals to directly derive a human-based POD. The main challenge is to derive a POD that most closely mimics one that would be selected in a regulatory assessment. Since regulatory PODs are intended to be protective of all adverse effects, the estimate should be at the lower end of the distribution of available PODs. Paul Friedman et al. (2020), for example, selected the 5th percentile of the distribution of *in vivo*

PODs. As shown in Figure S1, we found that their choice of the 5th percentile is a fairly accurate surrogate for regulatory PODs, with a median interquartile range ratio of 1 [0.83, 1.19], though with wide tails (geometric standard deviation, $GSD = 2.8$), and adopted this choice in our hierarchy.

If for a given chemical there are also no experimental animal data available, then we estimate PODs from New Approach Methods (NAMs), such as *in vitro* and *in silico* models. There has been much interest in using high-throughput *in vitro* screening data as surrogates for *in vivo* experimental animal data (e.g. Paul Friedman et al. 2020, Wang 2018, Wetmore et al. 2013), but the predictive power of *in vitro*-based NAMs in terms of PODs is still lacking. For instance, although Paul Friedman et al. (2020) suggest that NAM-based PODs may serve as 'conservative' surrogates of traditional PODs, their actual correlation is quite poor with $R^2 \leq 0.02$ (see Figure S2). On the other hand, the Conditional Toxicity Value (CTV) predictor Quantitative Structure-Activity Relationship (QSAR) model developed by Wignall et al. (2018) was specifically designed to predict regulatory PODs based on chemical structure, and has been demonstrated to make more accurate and precise regulatory POD predictions than other NAM-based methods. We extended this comparison to the traditional PODs analyzed by Paul Friedman et al. (2020), finding that the QSAR-based predictions of *in vivo* PODs are not only less biased, with ratios to traditional values closer to one, but also have greater precision, with typical errors less than one order of magnitude and $R^2 \sim 0.3$ (see Figure S3).

If a given chemical is outside of the domain of applicability of CTV, we obtain a NOAEL as POD through use a Threshold of Toxicological Concern (TTC), multiplied by a factor of 100 in order to "undo" the uncertainty factor already included in the TTC (Kroes et al. 2005). TTCs are used as a last resort because there are only three generic values to choose from, representing different Cramer classes (low, intermediate, and significant toxicity), and are intentionally 'conservative' estimates of the *in vivo* POD (Kroes et al. 2004). Thus, TTC-based PODs are flagged to facilitate sensitivity analysis as to the impact of their inclusion or exclusion.

After PODs are identified based on our suggested data selection hierarchy, auxiliary information in addition to the POD values themselves must be considered in order to derive appropriate dose-response factors. The full meta-data needed are listed in Tables S4 and S5.

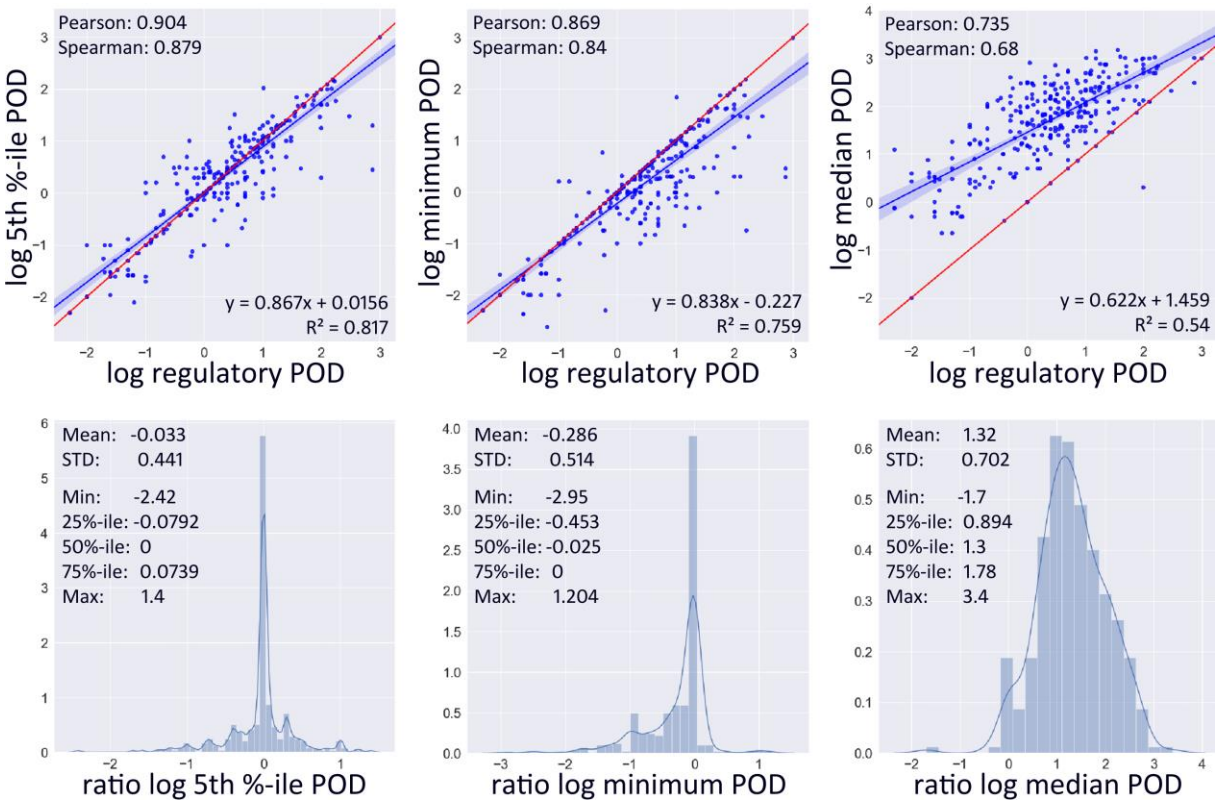

Figure S1. Comparison of various statistics of the *in vivo* point of departure (POD) distributions from Paul Friedman et al. (2020) with regulatory (conditional toxicity value, CTV) PODs compiled by Wignall et al. (2018). For Pearson and Spearman rank correlations, all *p*-values are $\ll 0.01$. Ratios of median interquartile ranges are obtained as log of 5th %-ile, minimum and median POD minus log of respective regulatory POD. All statistics refer to log scale data.

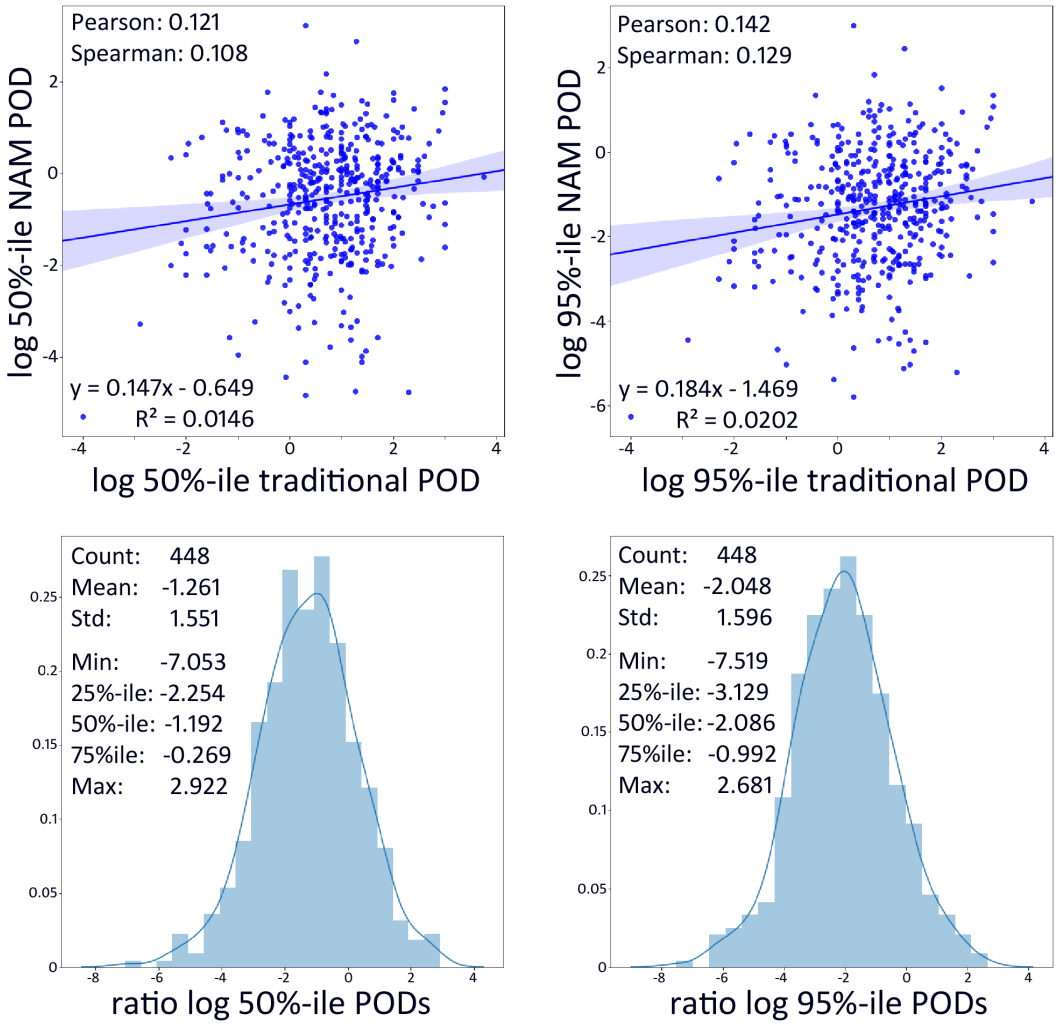

Figure S2. Comparison between 50th and 95th %-iles of new approach method (NAM) point of departure (POD) and traditional POD from Paul Friedman et al. (2020). For Pearson and Spearman rank correlations, all p-values are < 0.05. Ratios of median interquartile ranges are obtained as log of 50th %-ile and 95th %-ile NAM POD minus log of respective traditional POD. All statistics refer to log scale data.

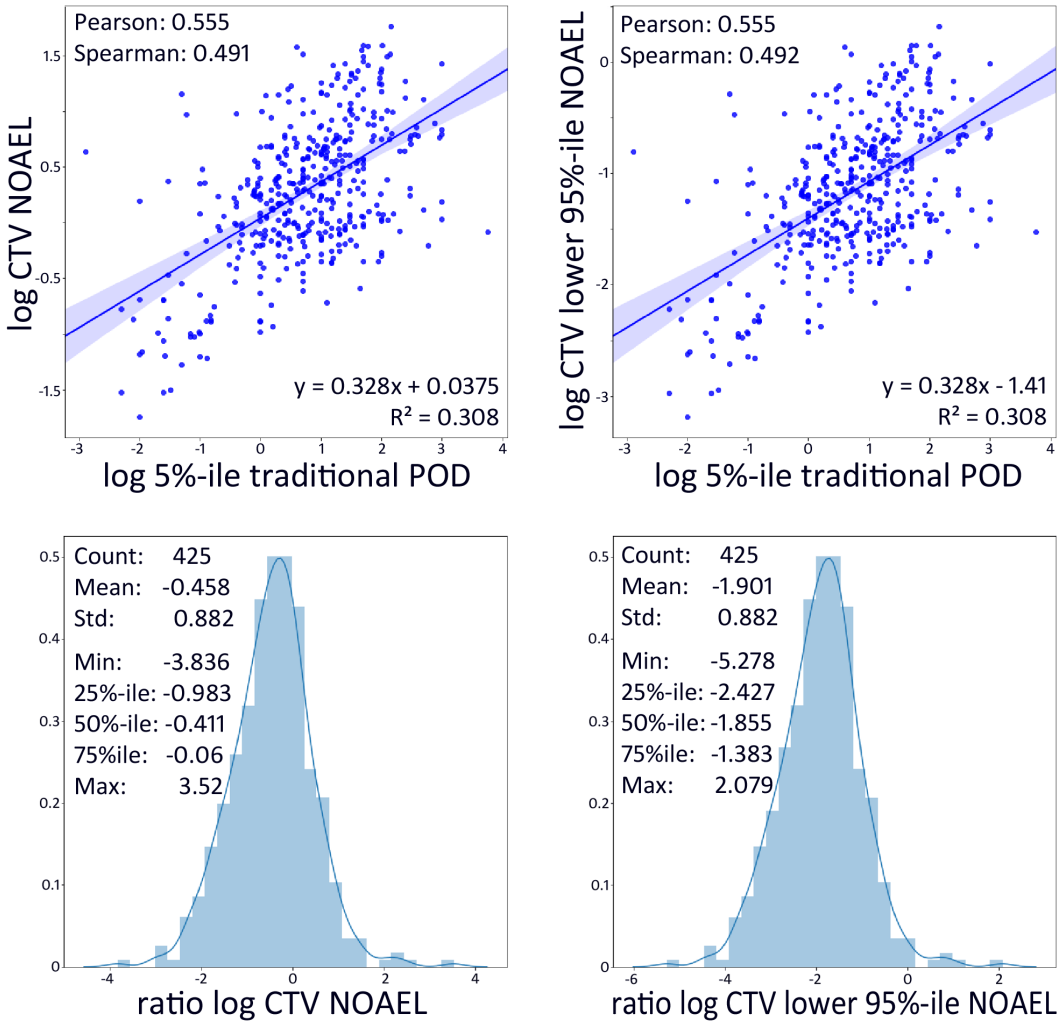

Figure S3. Comparison between conditional toxicity value (CTV) predictions from Wignall et al. (2018) and traditional points of departure (POD) from Paul Friedman et al. (2020). For Pearson and Spearman rank correlations, all p-values are $\ll 0.01$. Ratios of median interquartile ranges are obtained as log of CTV NOAEL and CTV lower 95th %-ile NOAEL minus log of respective traditional POD. All statistics refer to log scale data.

S-3b Hierarchy of toxicity data sources

As an example for U.S.-based regulatory values, we followed the hierarchy of data sources for deriving a suitable point of departure (POD) developed by Wignall et al. (2014, 2018):

1. U.S. Environmental Protection Agency (EPA) Office of Pesticide Programs (for pesticides only)
2. U.S. EPA Integrated Science Assessments and Integrated Risk Information System (IRIS) toxicological reviews
3. Centers for Disease Control and Prevention (CDC)/Agency for Toxic Substances and Disease Registry (ATSDR) toxicological profiles

4. U.S. EPA Provisional Peer Reviewed Toxicity Values (PPRTV)
5. U.S EPA Health Effects Assessment Summary Tables (HEAST)
6. Other U.S. EPA offices

S-3c Meta-data for identifying points of departure (POD)

Table S4. Documentation requirements for regulatory toxicity values and experimental studies. Table adapted from Chiu et al. (2018).

All PODs: • Chemical identification (name, CAS RN). • Source • Point of departure type [e.g. LOAEL, NOAEL, BMDL] and units [e.g. mg/kg-d]. - If NAM or TTC, assumed to be a NOAEL. - For BMDLs, benchmark response (BMR) and (if reported) BMD. - Type of effect (standardized to categories in Table S5) and (if reported) type of data (continuous or dichotomous). If NAM or TTC, assumed to be continuous effect with category "other." - For continuous effects with a BMDL based on 1 standard deviation (SD) change, data on control animals (number of animals, the mean and SD or SE response).
For experimental animal or regulatory toxicity values, also: • Species and (if reported) body weight.
For regulatory toxicity values, also: • Source and reported value of reference dose (RfD). • Individual uncertainty factors (UFs) (animal-to-human, human variability, subchronic-to-chronic, LOAEL-to-NOAEL, database) and composite UF.

Table S5. Standardized effect categories. Table adapted from Chiu et al. (2018).

• body weight • clinical chemistry • enzyme activity • food and/or water consumption • hematology • neurotransmitter • organ weight • urinalysis • clinical signs • gross pathology • mortality/survival • non-neoplastic histopathology • development • multiple • neuro behavior • none • other • reproduction

Table S6. Conceptual models and magnitudes of effect for different types of effects/endpoints. Table adapted from Chiu et al. (2018).

Continuous endpoints (response is variable, e.g. weight loss)
• **Description:** Used when the endpoint is reported as a continuous measurement. • **Effect categories included:** body weight, clinical chemistry, development (e.g. foetal weights), enzyme activity, food and/or water consumption, hematology, neuro-behavior (e.g. grip strength), neurotransmitter (e.g. cholinesterase inhibition), organ weight, reproduction (e.g. sperm counts), urinalysis. Most NAM approaches and TTC would be assumed to fall into this category. • **Magnitude of effect:** If a % change is reported, then that value is used. In cases where BMD modelling is used and a 1 SD change from the control group mean is reported, the 1 SD change is converted to a % change based on the reported SD in the control group. This change is made so that the BMD is interpretable as a magnitude of effect in humans. If only NOAELs or LOAELs are reported, it is adjusted to an equivalent BMD for a 5% change. Most NAM approaches and TTC would be assumed to be a surrogate for a NOAEL.
Dichotomous endpoints (yes/no response, e.g. cancer)
Quantal-deterministic (dichotomous) endpoints (response proportional to dose, e.g. alcohol intoxication)
• **Description:** Used when the endpoint is reported as incidence (number or fraction affected), but is judged to reflect an underlying (unreported) continuous endpoint that has been dichotomized using a cut-point; for the purposes of dose–response data analysis, the dose corresponding to a 50% "response" (e.g., a BMD_{50}, where 50% of the individuals are affected) from the incidence data would be used to estimate the dose at which the underlying continuous response crosses the cut-point (see WHO (2014) and Chiu and Slob (2015) for detailed discussions of this point). • **Effect categories included:** clinical signs, gross pathology, neuro-behavior (e.g. ataxia), non-neoplastic histopathology. • **Magnitude of effect:** Reflected in the severity of the effect for which the incidence is reported. If the BMD_{50} for incidence is reported, it is used. Otherwise, the reported POD is adjusted to the BMD_{50} (see Table S7).
Quantal-stochastic (dichotomous) endpoints (probability of response is proportional to dose, e.g. cancer)
• **Description:** Used when the endpoint is reported as a dichotomous measurement (i.e. as incidence), but is judged to reflect a stochastic process so that the incidence is an estimate of the probability of the effect occurring at the individual level. • **Effect categories included:** Mortality/survival, development (e.g. skeletal variations), reproduction (e.g. conception rate). • **Magnitude of effect:** If an extra risk value is reported (e.g. 5% extra risk), it is used. Otherwise, the reported POD (i.e. NOAELs or LOAELs) is adjusted to an equivalent BMD for a 10% extra risk (see Table S7).
Multiple endpoints
• For reproductive or developmental endpoints that do not specify a continuous or dichotomous measure (e.g. reported as NOAEL), both "Continuous" and "Quantal-Stochastic" models are implemented, reflecting both possibilities. • For non-reproductive and non-developmental endpoints that do not specify a continuous or dichotomous measure (e.g. reported as NOAEL), both "Continuous" and "Quantal-Deterministic" models are implemented, reflecting both possibilities.

Table S7. Extrapolation factors, uncertainty distributions assigned for POD and uncertainty factors. Table adapted from Chiu et al. (2018).

NOAEL to BMD extrapolation (ef_{BMD} in main text, eq. 24)
• **Purpose:** Adjusts for uncertainty due to use of NOAEL instead of a BMD, based on historical data (i.e. what range of BMD might occur given particular NOAEL). Used only if POD is LOAEL or NOAEL. • **Value:** Lognormal distribution (from WHO 2014), with P50=median and P95=95% probability

- Continuous endpoint, non-developmental study: P50=1/3, P95/P50=4.7
- Continuous endpoint, developmental study: P50=1/3 (i.e. BMD = NOAEL/(1/3) = NOAEL×3), P95/P50=7
- Quantal-deterministic endpoint: P50=2/9, P95/P50=5
- Quantal-stochastic endpoint: P50=2/3, P95/P50=4.7

LOAEL to NOAEL extrapolation
(If POD is LOAEL, first extrapolate to NOAEL, then apply NOAEL to BMD extrapolation)

- **Purpose:** Adjusts from LOAEL to NOAEL on a study-specific basis, including uncertainty. Used only if POD is LOAEL. WHO (2014) did not attempt to estimate this distribution from historical data because such data largely reflect dose spacing. It was therefore assumed that the reported UF_L reflected a "best estimate" of this factor. Since choices for this factor typically vary by 3-fold (e.g. 1, 3, or 10), the uncertainty was assigned this value.
- **Value:** Lognormal distribution, P50 = reported value for UF_L or expert judgment based on study; P95/P50=3

BMDL to BMD extrapolation (ef_{BMD} in main text, eq. 24)

- **Purpose:** Accounts for uncertainty in the BMD. For quantal-deterministic endpoints, additional adjustment from reported BMD to BMD_{50}. Used only if POD is BMDL.
- **Value:** Lognormal distribution (from WHO 2014)
  - If BMDU is reported, P50 = $(BMDL \times BMDU)^{0.5}$ and P95/P50 = $(BMDU/BMDL)^{0.5}$
  - If BMD, but not BMDU, is reported, P50=BMD, P95/P50=BMD/BMDL
  - If neither BMDU nor BMD not reported, P50=BMDL×3, P95/P50=3
  - Quantal-deterministic endpoints, if BMD_{50} not reported: BMD at the reported benchmark response (BMR) is multiplied by an additional factor of 3; additional uncertainty through adding 1.5^2 to $(P95/P50)^2$

Additional new approach method (NAM) extrapolation
(Used only when POD is based on NAM, in addition to above extrapolation steps)

- **Purpose:** Accounts for additional uncertainty due to use of NAM
- **Value:** Lognormal distribution with specified P50 and P95/P50 based on analysis (e.g. comparisons to regulatory values) or expert judgment

Exposure duration extrapolation (ef_t in main text, eq. 25)

- **Purpose:** Accounts for uncertainty in using a less than chronic study (e.g. subchronic, subacute, etc.) instead of a chronic one. Used only if endpoint is from a less than chronic study
- **Value:** Lognormal distribution (from WHO 2014)
  - Subchronic: P50=2, P95/P50=4
  - Subacute: P50=5, P95/P50=8

Interspecies dosimetric adjustment factor (ef_{BW} in main text, eq. 25)

- **Purpose:** Accounts for average interspecies differences due to allometry (oral) or respiratory tract geometry (inhalation).
- **Value:** Lognormal distribution (from WHO 2014)
  - Oral: $P50=(BW_{human}/BW_{animal})^{0.3}$, $P95/P50=(BW_{human}/BW_{animal})^{0.04}$; BW_{human} = 70 kg, BW_{animal} depends on species, from US-EPA (1988)
  - Inhalation: Use appropriate point value of dosimetric adjustment factor (DAF) based on Reactivity/Solubility (US-EPA 1994), without uncertainty

Interspecies toxicokinetics (TK) and toxicodynamics (TD) uncertainty (ef_{TKTD} in main text, eq. 25)

- **Purpose:** Accounts for chemical-specific interspecies TK and TD differences after accounting for interspecies BW scaling.
- **Value:** Lognormal distribution (from WHO 2014), P50=1, P95/P50=3

Human variability at 10% response-level extrapolation ($ef_{H,I=0.1}$ in main text, eq. 26)

- **Purpose:** Accounts for variability in sensitivity between the median human and the I^{th} %-ile human.
- **Value:** Lognormal distribution (from WHO 2014), for I=10%, P50=3.49, P95/P50=2.24

S-3d Uncertainty of dose-response relationship

In recognition of the uncertainties in both the population dose-response relationship as well as the appropriate point at which to evaluate it, we take the approach to select a metric that is "representative" of the range of possible values, but is also straight-forward to calculate. We ultimately chose the slope of the line from the 10% human population response, i.e. $DRF = 0.1/\mathrm{DLT10}$ (see main text, eq. 28), as the "representative" marginal slope for three main reasons. First, it is easily calculated using existing tools. Second, it represents a conceptually similar method as the original LCIA approach to take the slope from the 50% response. Finally, and most importantly, we found that the slope calculated from the 10% response is within the confidence interval for the marginal slope across exposure levels corresponding to a wide range of 'background' incidence levels. In Figure S4, we compare the median estimate and 90% confidence interval for the linearly extrapolated slope from the 10% response with the confidence intervals for the marginal slope at various levels of response for 81 chemicals used in the rice case study. This analysis shows that the median estimate of the linear slope is within the 95% confidence interval for the marginal slope from incidence levels of 0.01% to 50%, and the 95% confidence interval of the linear slope includes the median estimate for the marginal slope across this entire range. Thus, given the uncertainties, the linear slope from the 10% response appears to adequately represent the range of possible marginal slopes.

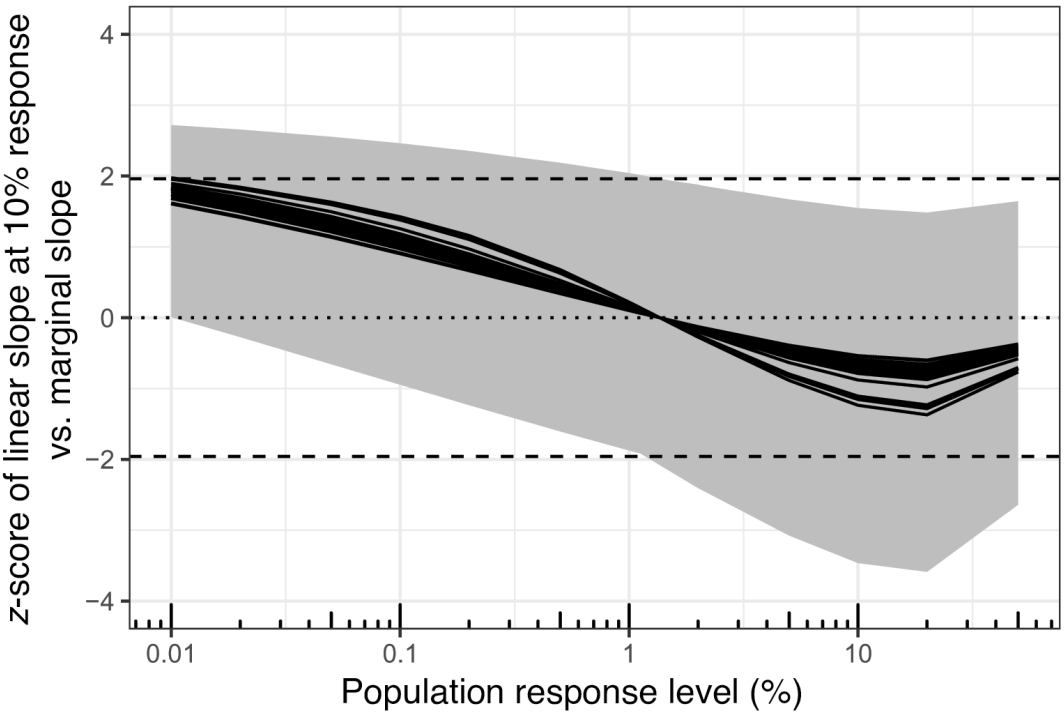

Figure S4. Comparison of confidence intervals for linear slope from 10% response to those for the marginal slope at varying levels of response across 81 chemicals. Lines (grey band)

represent the median (95% confidence interval) for the linear slope at a 10% response. Values on the x-axis are the population incidence levels at which the marginal slope is calculated, and the y-axis represents the *z*-score for the linear slope at a 10% response. Dashed line represents the 95% confidence interval for the marginal slope.

S-3e Severity factors

Table S8. Incidence-weighted DALY/incidence values for all cancer endpoints, reproductive/developmental endpoints, and all other non-cancer effects, based on data from Huijbregts et al. (2005).

Disease Category	DALY/incidence [years]	Estimated uncertainty*
Cancer effects	11.5	2.8-fold
Reproductive/developmental effects**	44.1	11-fold
Other non-cancer effects	2.4	6.5-fold

*Unitless, square root of the ratio of the weighted 97.5th %-ile to 2.5th %-ile of the contributing condition DALYs. Value for cancer directly applied and calculated from subsets as presented in Table 2 of Huijbregts et al. (2005).
**Denoted in Huijbregts et al. (2005) as “congenital anomalies”.

S-4 Rice case study

We applied the update near-field/far-field USEtox exposure assessment framework in a life cycle assessment (LCA) case study on rice production and consumption along three scenarios (China, India and U.S.-Switzerland). The functional unit was chosen to be 1 kg of cooked white rice consumed at home, and the full system description and life cycle inventory of this case study are described elsewhere (Frischknecht et al. 2016). In addition, rice packaging was included into the three scenarios as presented in Table S9.

For the rice case study, emission inventory data for the 115 chemicals identified along the rice cradle-to-gate for the three considered scenarios, the contribution of rice packaging manufacturing and disposal on the emission inventory, mass content of the six chemicals identified as constituents in rice packaging, related emission-based human intake fractions and product intake fractions, as well as human toxicity effect factors combining dose-response information and effect severity are summarized in Table S10, provided in a separate file.

Table S9. Specification of rice packaging for the three rice case study scenarios. Weight fractions of chemicals in packaging material are based on Biryol et al. (2017, Table S3).

Scenario	**China (CN)**	**India (IN)**	**U.S.-Switzerland (US/CH)**
Rice packaging	1 recycled cardboard package for storing 1000 g white rice; packaging mass: 37 g; packaging area: 750 cm²	1 low-density polyethylene (LDPE) package for storing 1000 g white rice; packaging mass: 10 g; packaging area: 670 cm²	*Outer package*: 1 recycled cardboard package; packaging mass: 37 g; packaging area: 750 cm². *Inner package*: 8 low-density polyethylene (LDPE) cooking bags for storing 125 g white rice each; packaging mass: 3.5 g/bag; packaging area: 300 cm²/bag
Storage conditions	2 months storage at 20 °C	2 months storage at 20 °C	2 months storage at 20 °C; *Inner package*: 20 minutes boiling at 100 °C
Packaging chemical ingredients	Diisobutyl phthalate (CAS 84-69-5), weight fraction: 0.53%; Dibutyl phthalate (CAS 84-74-2), weight fraction: 0.91%; Diisopropylnaphthalene (CAS 38640-62-9), weight fraction: 0.53%	Laurolactam (CAS 947-04-6), weight fraction: 0.53%; Acetyltributylcitrate (CAS 77-90-7), weight fraction: 0.53%; Butylhydroxytoluene (CAS 128-37-0), weight fraction: 0.53%	*Outer package*: chemical ingredients as in CN scenario; *Inner package*: chemical ingredients as in IN scenario

Human toxicity dose-response factors (*DRF*) used as input to calculate human toxicity effect factors for all chemicals considered in the rice case study are presented for ingestion (oral) exposure in Figure S5 and for inhalation exposure in Figure S6.

Figure S5. Ingestion (oral) exposure dose-response factors (*DRF*) for chemicals evaluated in the rice case study.

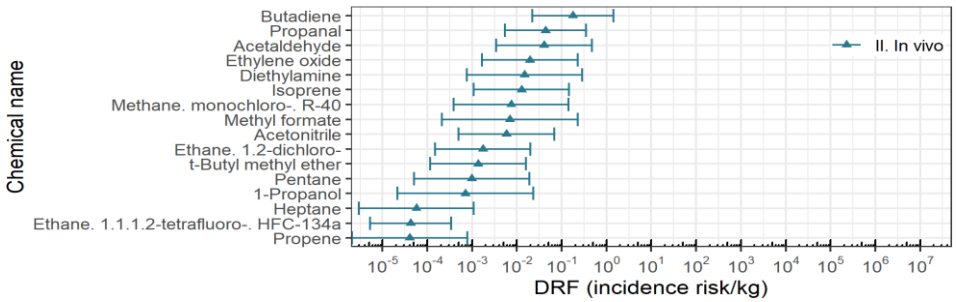

Figure S6. Inhalation exposure dose-response factors (*DRF*) for chemicals evaluated in the rice case study.

Final inventory and impact characterization results for the rice case study are summarized in Figure S7. Life cycle inventory, human exposure (expressed as intake and product intake fractions), toxicity effect factors, and impact scores for 6 chemicals found in rice packaging (top 6 chemicals) and for chemical cradle-to-gate emissions (all other chemicals) of the rice case study in China (CN), India (IN) and U.S./Switzerland (US/CH). Contribution bars in all plots are shown for the US/CH scenario. Dash symbols denote the contribution of rice packaging manufacturing and disposal as compared to the total cradle-to-gate. (a) **Life cycle inventory**: kg in rice package/functional unit and contribution of packaging material (top 6 chemicals); kg emitted/functional unit and contribution of emission compartments (all other chemicals). (b) **Human exposure**: kg intake/kg in rice packaging material (top 6 chemicals) and kg intake/kg emitted (all other chemicals) aggregated over all contributing exposure routes, and contribution of exposure route. (c) **Toxicity effects**: DALY/kg intake, combining dose-response and effect severity, aggregated over and contribution of cancer, reproductive/developmental, and other non-cancer effects. (d) **Impact scores**: DALY/functional unit and contribution to household population versus product users (top 6 chemicals); DALY/functional and contribution of emission compartments (all other chemicals).

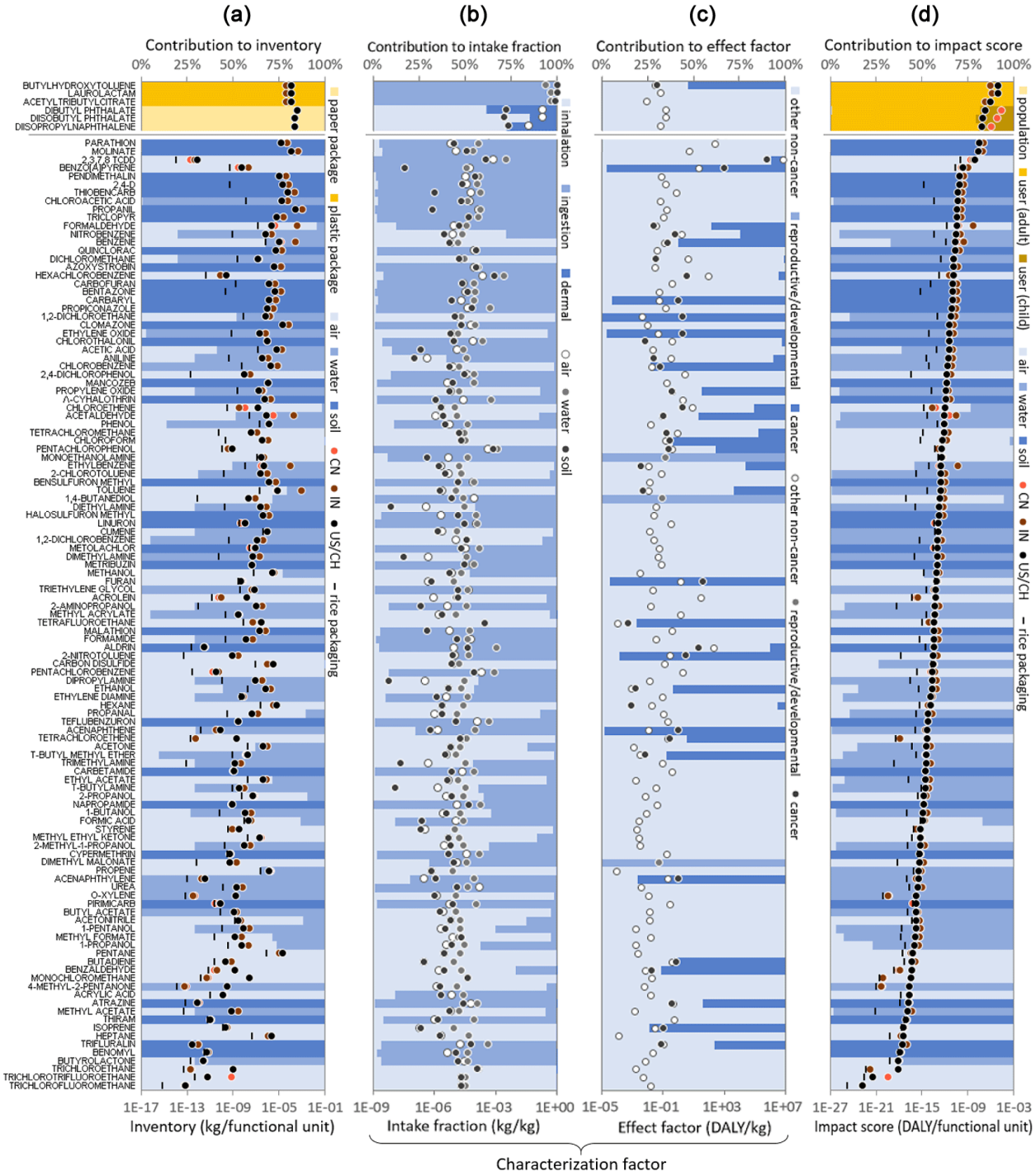

Figure S7. Combined bar and scatter plots summarizing rice case study life cycle inventory and toxicity characterization results.

References

Biryol D et al. (2017): High-throughput dietary exposure predictions for chemical migrants from food contact substances for use in chemical prioritization. Environment International 108: 185-194

Bremmer HJ et al. 2006: Cosmetics Fact Sheet to assess the risks for the consumer. Updated version for ConsExpo 4. RIVM report 320104001/2006, National Institute for Public Health and the Environment, Bilthoven, The Netherlands

Chiu WA, Slob W (2015): A unified probabilistic framework for dose-response assessment of human health effects. Environmental Health Perspectives 123: 1241-1254

Chiu WA et al. (2018): Beyond the RfD: Broad application of a probabilistic approach to improve chemical dose-response assessments for noncancer effects. Environmental Health Perspectives 126: 1-14

Cox SS et al. (2002): Predicting the emission rate of volatile organic compounds from vinyl flooring. Environmental Science and Technology 36: 709-714

Csiszar SA et al. (2016): High-throughput exposure modeling to support prioritization of chemicals in personal care products. Chemosphere 163: 490-498

Csiszar SA et al. (2017): Stochastic modeling of near-field exposure to parabens in personal care products. Journal of Exposure Science and Environmental Epidemiology 27: 152-159

Earnest CM, Corsi RL (2013): Inhalation exposure to cleaning products: Application of a two-zone model. Journal of Occupational and Environmental Hygiene 10: 328-335

Fantke P et al. (2020): Toward effective use of REACH data for science and policy. Environment International 135: 105336

Frischknecht R et al. (2016): Global guidance on environmental life cycle impact assessment indicators: Progress and case study. The International Journal of Life Cycle Assessment 21: 429-442

Huang L et al. (2017): A quantitative property-property relationship for the internal diffusion coefficients of organic compounds in solid materials. Indoor Air 27: 1128-1140

Huang L, Jolliet O (2019a): A quantitative structure-property relationship (QSPR) for estimating solid material-air partition coefficients of organic compounds. Indoor Air 29: 79-88

Huang L, Jolliet O (2019b): A combined quantitative property-property relationship (QPPR) for estimating packaging-food and solid material-water partition coefficients of organic compounds. Science of The Total Environment 658: 493-500

Huijbregts MAJ et al. (2005): Human-toxicological effect and damage factors of carcinogenic and noncarcinogenic chemicals for life cycle impact assessment. Integrated Environmental Assessment and Management 1: 181-244

Isaacs KK et al. (2014): SHEDS-HT: An integrated probabilistic exposure model for prioritizing exposures to chemicals with near-field and dietary sources. Environmental Science and Technology 48: 12750-12759

Kroes R et al. (2004): Structure-based thresholds of toxicological concern (TTC): Guidance for application to substances present at low levels in the diet. Food and Chemical Toxicology 42: 65-83

Kroes R et al. (2005): The threshold of toxicological concern concept in risk assessment. Toxicological Sciences 86: 226-230

Little JC et al. (2012): Rapid methods to estimate potential exposure to semivolatile organic compounds in the indoor environment. Environmental Science and Technology 46: 11171-11178

Meesters JAJ et al. 2018: Cleaning Products Fact Sheet : Default parameters for estimating consumer exposure - Updated version 2018, National Institute for Public Health and the Environment, Bilthoven, The Netherlands

Paul Friedman K et al. (2020): Utility of *in vitro* bioactivity as a lower bound estimate of *in vivo* adverse effect levels and in risk-based prioritization. Toxicological Sciences 173: 202-225

Rosenbaum RK et al. (2011): USEtox human exposure and toxicity factors for comparative assessment of toxic emissions in life cycle analysis: Sensitivity to key chemical properties. The International Journal of Life Cycle Assessment 16: 710-727

Rosenbaum RK et al. (2015): Indoor air pollutant exposure for life cycle assessment: Regional health impact factors for households. Environmental Science and Technology 49: 12823-12831

Sobanska M, Le Goff F (2014): IUCLID (International Uniform Chemical Information Database). In: Wexler P (Editor), Encyclopedia of Toxicology, 3rd Ed. Academic Press, Oxford, pp. 3-5

ten Berge W (2009): A simple dermal absorption model: Derivation and application. Chemosphere 75: 1440-1445

US-EPA United States - Environmental Protection Agency 1988: Recommendations for and documentation of biological values for use in risk assessment, United States - Environmental Protection Agency, Washinton, D.C.

US-EPA United States - Environmental Protection Agency 1994: Methods for derivation of inhalation reference concentrations (RfCs) and application of inhalation dosimetry, United States - Environmental Protection Agency, Washington, D.C.

US-EPA United States - Environmental Protection Agency 2011: Exposure Factors Handbook: 2011 Edition, Office of Research and Development, National Center for Environmental Assessment, Washington, D.C.

Wang D (2018): Infer the in vivo point of departure with ToxCast in vitro assay data using a robust learning approach. Arch Toxicol 92: 2913-2922

Wenger Y et al. (2012): Indoor intake fraction considering surface sorption of air organic compounds for life cycle assessment. The International Journal of Life Cycle Assessment 17: 919-931

Wetmore BA et al. (2013): Relative impact of incorporating pharmacokinetics on predicting *in vivo* hazard and mode of action from high-throughput *in vitro* toxicity assays. Toxicological Sciences 132: 327-346

WHO World Health Organization 2014: Guidance document on evaluating and expressing uncertainty in hazard characterization, World Health Organization, Geneva, Switzerland

Wignall JA et al. (2014): Standardizing benchmark dose calculations to improve science-based decisions in human health assessments. Environmental Health Perspectives 122: 499-505

Wignall JA et al. (2018): Conditional toxicity value (CTV) predictor: An *in silico* approach for generating quantitative risk estimates for chemicals. Environmental Health Perspectives 126: 057008

Williams AJ (2011): Chemspider: A platform for crowdsourced collaboration to curate data derived from public compound databases. In: Ekins S et al. (Editors), Collaborative Computational Technologies for Biomedical Research. John Wiley and Sons, Hoboken, New Jersey, pp. 363-386

Williams AJ et al. (2017): The CompTox Chemistry Dashboard: A community data resource for environmental chemistry. Journal of Cheminformatics 9: 61